RSC Advances

PAPER

View Article Online
View Journal | View Issue

Cite this: *RSC Adv.*, 2024, **14**, 2070

Influence of barium substitution on the physical, thermal, optical and luminescence properties of Sm^{3+}-doped metaphosphate glasses for reddish orange light applications

Hounaida Mrabet,*[a] Ismail Khattech,[a] Souhir Bouzidi,[b] Lilia Kechiche,[c] A. Jbeli,[d] Nuha Al Harbi,[e] Chaker Bouzidi,[f] Francisco Muñoz[g] and Rolindes Balda[hi]

Received 22nd November 2023
Accepted 6th December 2023

DOI: 10.1039/d3ra08015c

rsc.li/rsc-advances

Our present study focuses on examining the thermal, structural and luminescent characteristics of sodium barium metaphosphate glasses doped with Sm^{3+}. Glass samples with molar compositions $(100 - y)[(50P_2O_5)-(50\text{-}xNa_2O)-(xBaO)]-ySm_2O_3$, where $x = 20$, 25, 30, 35, 40 and $y = 0.3$ and 1% were first synthesized by conventional melt quenching and later dehydroxylated under a constant N_2 flow to ensure final glasses with a very high degree of chemical and optical homogeneity and free of water. Upon the addition of BaO and Sm_2O_3, refractive index, molar mass, density, glass transition temperature and dilatometric softening temperature exhibited an increase, whereas the coefficient of thermal expansion showed a decrease. The FTIR spectra analysis reveals a network depolymerization that intensifies with rising BaO concentration, ultimately transitioning from a modifier oxide to a glass-forming element, at higher BaO concentrations. All doped samples exhibited prominent absorption bands in the visible (VIS) and near-infrared (NIR) regions, as revealed by the optical absorption spectra. The Na_2O modifier demonstrated greater influence on Sm^{3+} emission compared to BaO, a phenomenon that can explained by the moderation of the local ligand field strength resulting from this substitution. With an increase in Sm_2O_3 concentration from 0.3 to 1 mol%, the experimental lifetimes of the $^4G_{5/2}$ level decrease, primarily attributed to the presence of energy transfer mechanisms. A discussion of Judd–Ofelt parameter analysis and glass radiation properties will be presented.

1. Introduction

Nowadays, optical materials based on trivalent lanthanide ions are being widely applied in various technological applications such as photonic displays, communications devices, laser materials, hole burning high-density memories, optical storage, *etc.*[1–6] Therefore, the special features of glassy matrices, such as low production cost, better thermal stability, mechanical strength, and chemical durability, make them more suitable as host materials than crystalline compounds. Phosphate-based glasses are recognized as significant materials in certain applications due to their favorable characteristics, including high solubility for rare-earth ions with minimal clustering effects, low melting temperature, low glass transition temperature, high thermal expansion coefficient, and biocompatibility.[7,8] Based on previous investigations,[9] the addition of barium oxide to phosphate glasses enhances thermal stability, the ability to form glass structures, and chemical resistance. It also reduces thermal expansion and phonon frequencies, thereby improving the internal quantum efficiency of luminescent materials. Barium-containing glass has been around since the earliest days of glass science, with a number of important applications such as its relevancy for making: materials to adapt optical properties, gamma ray shielding materials, barrier of plasma display ribs,[10] sulphate-bearing high level liquid waste,[11] and gamma ray shielding.[12,13] Barium phosphates, whether in crystalline or glassy form, are

[a]*Chemistry Department, Université de Tunis El Manar, Faculty of Science, Materials Crystal Chemistry and Applied Thermodynamics Laboratory LR15SE01, Tunisia. E-mail: hounaida.mrabet31@gmail.com*

[b]*Département de Physique, Laboratoire de la Matière Condensée et des Nanosciences, Faculté des Sciences de Monastir, Avenue de l'Environnement Monastir, 5019 Monastir, Tunisia*

[c]*Department of Science and Technology, University College of Ranyah, Taif University, P.O. Box 11099, Taif 21944, Saudi Arabia*

[d]*Department of Information Systems, College of Computer and Information Sciences, Majmaah University, Al-Majmaah 11952, Kingdom of Saudi Arabia*

[e]*Departement of Physics Faculty of Applied Sciences, Umm Al-Qura University, Makkah, Saudi Arabia*

[f]*Physical Chemistry Laboratory for Mineral Materials and Their Applications, National Center for Research in Materials Sciences, Borj Cedria Technopark, Tunisia*

[g]*Institute of Ceramics and Glass (CSIC), Madrid, Spain*

[h]*Applied Physics Department, Faculty of Engineering, University of the Basque Country UPV/EHU, Bilbao, Spain*

[i]*Materials Physics Centre CSIC-UPV/EHU, San Sebastian, Spain*

significant in photonic applications when doped with rare-earth or transition metal ions. Additionally, the addition of small quantities of barium oxide or barium sulfate to the composition of bioactive materials imparts radio-opacity to the implants.[11] RE^{3+} ions doped phosphate glasses were used in optical fibres,[14] vitrification of radio-active waste,[15] tissue engineering[16] and many other applications. The Sm^{3+} ion is well suited for doping due of their excited energy level $^4G_{5/2}$ level which shows greater quantum efficiency with various quenching emission channels,[17] and presents strong reddish-orange emission, owns sufficient energy to provoke photodynamic reaction. The reddish light region is highly effective at penetrating human tissue 50 to 200% more deeply than blue or green light. Therefore, glasses doped with Sm^{3+} ions could find applications in high-power laser sources emitting reddish-orange light for the treatment of cancer. Additionally, the effective energy gap of Sm^{3+}-doped glass at 560 nm has various applications in daytime running lights and traffic signals. Consequently, the Sm^{3+} ion was chosen as the doping element for the current work. Recently, Naick *et al.* investigated the optical absorption spectra of trivalent samarium ions doped phosphate glasses with Li_2O, MgO, CaO, SrO and BaO as modifiers for visible orange-red photonic domains.[18] Several researchers have explored different optical absorption analysis of phosphate and sulfophosphate glasses doped with Sm^{3+} ions.[19] It has been observed that within these glass matrices, there is a conversion of oxygen atoms from bridging to non-bridging positions. Hence, in this present work, we prepared Na_2O–BaO–P_2O_5 glasses doped with 0.3 and 1.0 mol% Sm_2O_3 by conventional melt quenching synthetic method. In glass compositions featuring network modifier ions with low field strength, an intriguing phenomenon emerges: the fluorescence lifetime of doped rare earth ions experiences a substantial enhancement as the concentration of network modifiers increases in both alkali and alkaline earth glasses.[20–22] This phenomenon underscores the pivotal role of the network modifier in influencing the optical behavior of rare earth-doped glasses. In our investigation, we specifically target the influence of BaO on the physical and optical attributes of glasses. Our primary focus lies in exploring the coordination dynamics between high field strength Na^+ and Ba^{2+} cations within glass networks. Understanding the impact of these two modifiers on the phosphate network is crucial as the spectroscopic properties of rare earth ions heavily rely on their local environment. Thus, altering the Sm^{3+} ions sites within the glass matrix could potentially intensify their emission. Through this exploration, we aim to uncover fundamental principles that not only enhance our comprehension of material properties but also offer potential insights for optimizing the optical characteristics, particularly in the context of reddish-orange laser applications.

2. Materials and methods

Glasses with composition $(1-y)((50-x)Na_2O$–$xBaO$–$50P_2O_5)$–ySm_2O_3, in mol% with $x = 20$, 25, 30, 35, 40 and $y = 0.3$ and 1, were obtained by melt and quenching from batches synthesized by mixing reagent grade chemicals, Na_2CO_3, $BaCO_3$, $(NH_4)_2HPO_4$, and Sm_2O_3. In the first step, the batches were placed in porcelaine crucibles and slowly calcined overnight up to 450 °C. Then, they were melted for 2 h at temperatures of 900–1100 °C depending on the composition. A second melting of each glass was performed to obtain homogeneous and dehydroxylated glasses. This last was performed on about 5 g of each original glass in a graphite crucible, using a constant nitrogen flow within a tube furnace and, in the present case, at 750 °C for 6 h, following the methodology described in a previously published procedure in ref. 23.

The FTIR spectra were recorded on PerkinElmer Spectrum 100 spectrometer between 750 and 5000 cm^{-1} on plane parallel square samples of about 1 cm^2 and between 1 and 2 mm thick. This analysis was performed to investigate the structural modifications resulting from changes in the glass composition and to evaluate the hydroxyl groups in the glasses before and after re-melting, thereby confirming the efficiency of our glass synthesis method. The density (ρ) of the glass compounds was measured at room temperature using the Archimedes principle, with ethanol as the immersion liquid. The molar volume (V_m) of glass samples was calculated dividing the molar mass of each composition by its density. The dilatometric softening point (T_d), glass transition temperature (T_g), and coefficient of thermal expansion (CTE) were measured from very small glass pieces using a differential dilatometer (Netzsch Gerätebau model 402 EP). Dilatometry measurements were performed in the temperature range of 20 to 680 °C at a heating rate of 10 °C min^{-1}. The refractive index (n) was measured at room temperature using an Abbe refractometer, with monobromonaphthalene serving as the contact liquid. The measurements were performed at a wavelength of 589 nm. The optical absorption spectra were captured in the ultraviolet, visible, and near-infrared (UV-Vis-NIR) region spanning from 200 to 2000 nm. A UV-Vis-NIR spectrophotometer (Shimadzu, UV-3600) was employed for this purpose. The emission spectra and lifetime were measured with a fluorescence spectrophotometer FS5, equipped with a 150 W Xenon lamp. Then, the emission was detected using a Hamamatsu R928P photomultiplier.

3. Results and discussion

To demonstrate the effectiveness of our glass synthesis method, we recorded FTIR spectra from 20BaSm1 glass sample before and after re-melting in the spectral range of 2600–5000 cm^{-1}, as shown in Fig. 1(a). It is worth noting that the spectra display a broad IR absorption band spanning from 2680 to 3400 cm^{-1}, which is likely attributed to P–O–H stretching vibrations. The decrease in this signal in the re-melted sample suggests the breakdown and disruption of hydroxyl groups in the glass. Moreover, in the range of 3450 to 3650 cm^{-1}, the OH stretching mode undergoes a substantial reduction upon re-melting the glass in a nitrogen (N_2) atmosphere. This observation further indicates a significant decrease in the water content of the glasses due to the thermal treatment under a continuous N_2 flow. Based on the FTIR measurements, the absorption coefficient of hydroxyl ions in the glasses, α_{OH} (cm^{-1}), was evaluated,

using eqn (1), following the methodology described in ref. 24 and 25.

$$\alpha_{OH} = -\log(T_{5000}/T_{3000})t \quad (1)$$

The results obtained were summarized in Table 1. The results indicate a reduction in the absorption coefficient of OH ions in the glass samples that underwent re-melting under a continuous N_2 flow at 750 °C for 6 hours. It's important to note that the dehydroxylation process is thermally activated, as evidenced by the consistent decrease in OH content. The dehydroxylation method through a second melting under N_2 has proven to be very effective in removing traces of water from the glasses as shown by the small OH absorption confidents at 3000 cm^{-1}.

Examining the FTIR spectra of BaSm-1 glasses within the 750–1350 nm range (Fig. 1(b)) provides valuable insights into the structural modifications resulting in the glass composition changes. The structural framework is predominantly characterized by the presence of PO_4 tetrahedral units, with its features notably influenced by the incorporation of BaO into the glass matrix. Within the spectra, a prominent band appearing around 890 cm^{-1}, indicating the asymmetric stretching vibration of P–O bonds, ν_{as} (P–O–P).[26,27] Around 1075 cm^{-1}, another significant band arises, though the specific vibrational mode of ν_s (P–O–P) of both Q^2 and Q^1 units.[28] The band at approximately 1250 cm^{-1} is associated with the asymmetric stretching vibration of P–O–P bonds, ν_{as} (P–O–P).[26] Between 950 and 1030 cm^{-1}, multiple shoulders are detected and they were assigned to ν_s (PO_3^{2-}) in Q^1 units.[29] According to the spectral data, an increase in the BaO content from 20 to 30 mol% results in a higher proportion of Q^2 units at the expense of Q^1 units. This can be confirmed from the increase in the band at 890 cm^{-1} with the reduction in the band at 1250 cm^{-1}. These findings suggest that the phosphate chain depolymerizes as BaO substitutes Na_2O content. As the barium content continues to increase, an inverse trend becomes apparent. This indicates that this element primarily serves as a modifier oxide only at relatively low concentrations, transitioning into a glass-forming element at higher concentrations. In this context, we are well-positioned to conduct an effective exploration of the spectroscopic features of RE elements, specifically Sm^{3+}, in response to variations in the degree of depolymerization and polymerization within the phosphate matrix.

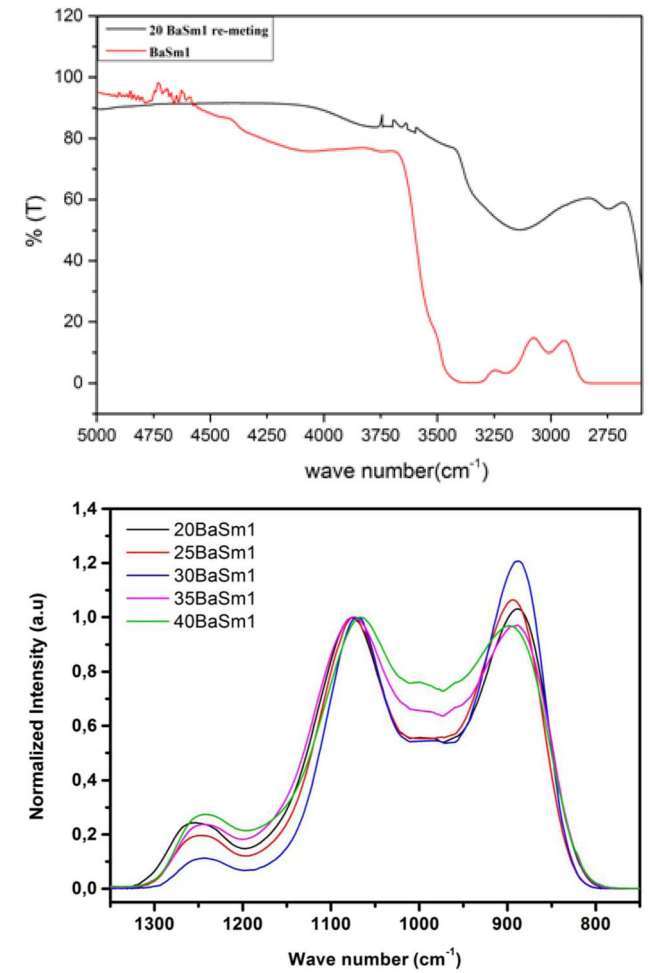

Fig. 1 FTIR spectra of the BaSm-1 glasses.

Table 1 Absorption coefficient of hydroxyl ions, α_{OH} (cm^{-1}), in the glasses before and after dehydroxylation

Glass	Density (g cm^{-3})	T_g (°C)	T_d (°C)	CTE (10^{-6} K^{-1})	Refractive index
20BaSm0.3	2.99	310.3	343.0	18.5	1.5275
25BaSm0.3	3.09	326.3	359.5	16.6	1.5379
30BaSm0.3	3.20	334.8	379.6	15.6	1.5465
35BaSm0.3	3.32	360.9	497.6	14.8	1.5589
40BaSm0.3	3.42	374.1	426	14.7	1.5738
20BaSm1	3.03	337.6	354.4	17.0	1.5197
25BaSm1	3.14	352.6	369.4	16.0	1.5429
30BaSm1	3.26	367.1	384.7	15.1	1.5509
35BaSm1	3.35	360.9	497.6	14.8	1.5595
40BaSm1	3.48	374.1	426	14.7	1.5739

Physical properties of series A, Na_2O–BaO–P_2O_5-0.3 Sm_2O_3 (BaSm-0.3) and series B, Na_2O–BaO–P_2O_5-1Sm_2O_3 (BaSm-1) of glasses are gathered in Table 2, density, dilatometric softening temperature, glass transition temperature, coefficient of thermal expansion and refractive index. The density and refractive index of the glass samples exhibit an increase as the BaO content increases. This can be attributed to the higher molar mass of BaO in comparison to Na_2O and the higher electronic density of Ba^{2+} ions compared to Na^+ ions. In agreement with FTIR analyses, these factors contribute to the hindrance of light waves passing through the glass samples.[11–30] The relationship between the refractive index of the glass and its density variation with BaO content is governed by the Lorentz–Lorentz equation.[31] This equation establishes a direct correlation between the refractive index and density of the glass.[11] The 1 to 2% difference in the values of the physical properties between the two sets of glasses can be explained by the mass percentage increase of samarium oxide. Table 2 presents the dilatometric softening temperature (T_d), coefficient

Table 2 Refractive index, density, glass transition temperature (T_g), dilatometric softening temperature (T_d) and coefficient of thermal expansion coefficient (CTE)

Glass sample	α_{OH} (cm^{-1}) As-prepared samples	α_{OH} (cm^{-1}) Re-melted sample
20BaSm0.3	2.88	0.86
25BaSm0.3	2.53	0.86
30BaSm0.3	2.93	0.91
35BaSm0.3	2.12	0.30
40BaSm0.3	2.76	0.84
20BaSm1	2.47	0.54
25BaSm1	2.61	0.74
30BaSm1	2.94	0.65
35BaSm1	2.75	0.52
40BaSm1	2.84	0.71

of thermal expansion (CTE) and glass transition temperature (T_g) values corresponding to different glass compositions. These data are also graphically illustrated in Fig. 2. Glass transition temperature of series A rises from 310 to for 374 °C for the glasses containing between 20 and 40 mol% of BaO and it is comprised between 337 and 390 °C in series B for similar contents of BaO. The dilatometric softening temperature exhibits a similar pattern of variation to that observed in the glass transition temperature across all the studied glass series. The coefficient of thermal expansion shows an opposite trend in the two glass series with a minimum of 14.7×10^{-6} K^{-1} for the compositions with 40 mol% BaO. The higher ionic field strength of Ba^{2+} modifier ions (0.49) compared to Na^{+} ones (0.19) strengthens the glass network through more covalent Ba–O–P bonds when Na_2O is systematically substituted by BaO, causing the observed increase in the T_g and T_d characteristic temperatures as well as the decrease in the CTE. The addition of a 1 mol% Sm_2O_3 instead of 0.3 in glasses of series B produces a similar effect on the thermal properties though minor increase in magnitude, with an increment of between 10 to 20 °C in the T_g values.

The UV-Vis-NIR absorption curves of series A and series B glasses are plotted in Fig. 3 and 4, respectively. From these spectra, it is evident that all glass samples exhibit 13 absorption bands that share the same characteristics, with the exception of variations in band intensities. Hence, in both series of glasses, the absorption bands are observed at specific wavelengths: 318, 333, 345, 361, 375, 402, 439, 480, 945, 1079, 1230, 1378, 1483, 1530 and 1589 nm, these bands correspond to transitions from the ground state $^6H_{5/2}$ to various excited states, including $^4P_{3/2}$, $^4G_{9/2}$, $^3H_{7/2}$, $^4D_{3/2,5/2}$, $^6P_{7/2}$, $^4F_{7/2}$ + $^6P_{3/2}$, $^4M_{17/2}$ + $^4G_{9/2}$ + $^4I_{9/2}$, $^4M_{11/2}$ + $^4I_{11/2,13/2}$, $^6F_{11/2}$, $^6F_{9/2}$, $^6F_{7/2}$, $^6F_{5/2}$, $^6F_{3/2}$, $^6H_{15/2}$ and $^6F_{1/2}$, respectively.[25,32] The Judd–Ofelt theory was employed to examine the spectroscopic properties of the glass samples. This involved calculating parameters such as the oscillator strength (f), radiative lifetime, J–O parameters (Ω_2, Ω_4, and Ω_6), radiative transition possibility (A_R), and branching ratio (β_R).[33] The calculated oscillator strength (f_{cal}) of an electric dipole–dipole absorption transition from the initial state (ψ_j) to the final state

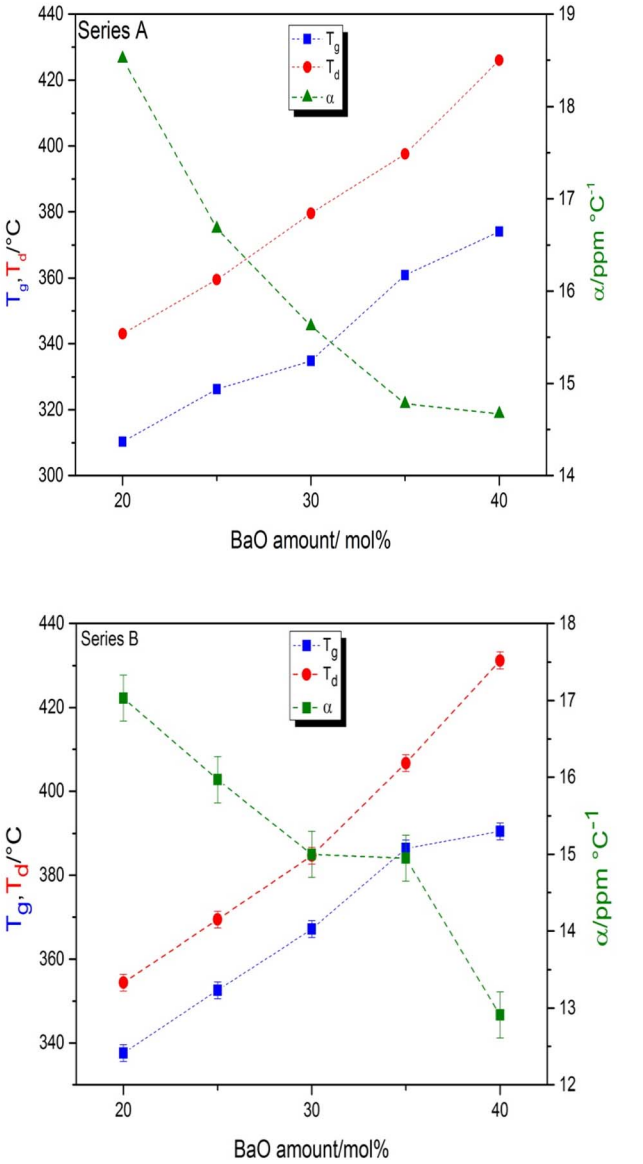

Fig. 2 Compositional dependence of glass transition temperature, T_g, dilatation softening temperature, T_d, and the coefficient of thermal expansion in the glass series A: Na_2O–BaO–P_2O_5–0.3Sm_2O_3 and in the glass series B: Na_2O–BaO–P_2O_5–1Sm_2O on the BaO content. The error in the values of T_g and T_d is smaller than the symbol size.

($\psi'_{j'}$) of depends on three Ω_λ parameters (λ = 2, 4 and 6) given by:[34]

$$f_{cal} = \left[\frac{8\pi mcv}{3h(2J+1)}\right]\left[\frac{(n^2+2)^2}{9n}\right] \times \sum_{\lambda=2,4,6} \Omega_\lambda (\psi J \| U\lambda \| \psi' J')^2 \quad (2)$$

where λ is the mean wavelength of the observed transition, m is the electron mass, n the refractive index, c is the light velocity, Ω_λ the JO parameters, $\|U^\lambda\|^2$ are the doubly reduced squared matrix elements of a unit tensor operator, which are considered from the intermediate coupling approximation for the transition from ψj to $\psi' j'$ and $(n^2 + 2)^2/9n$ is the Lorentz local field correction factor. The experimental oscillator strength (f_{exp}) of

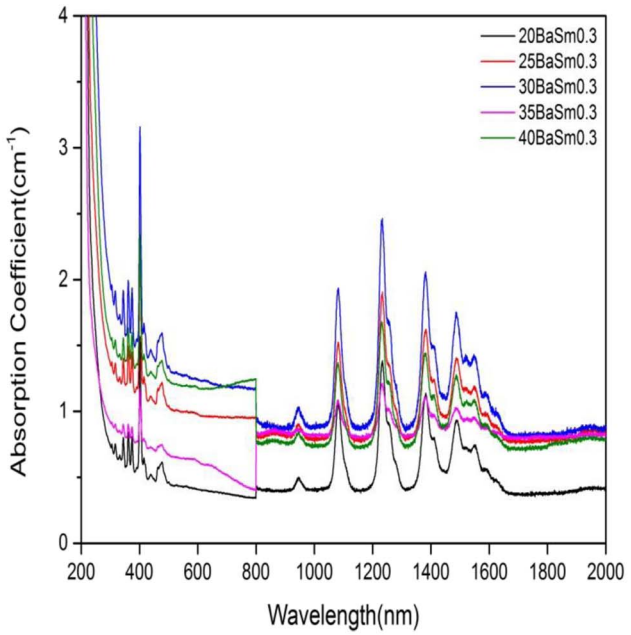

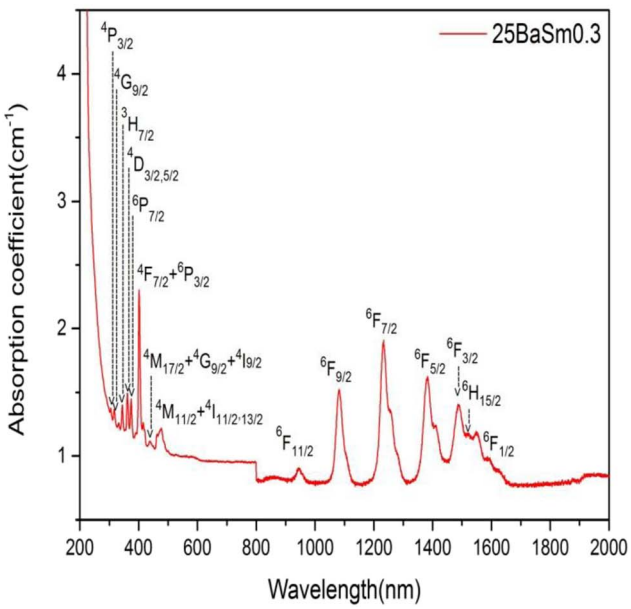

Fig. 3 The absorption spectra of series A glasses for (a) all concentrations and (b) 25 mol% of BaO and 0.3 mol % of Sm_2O_3.

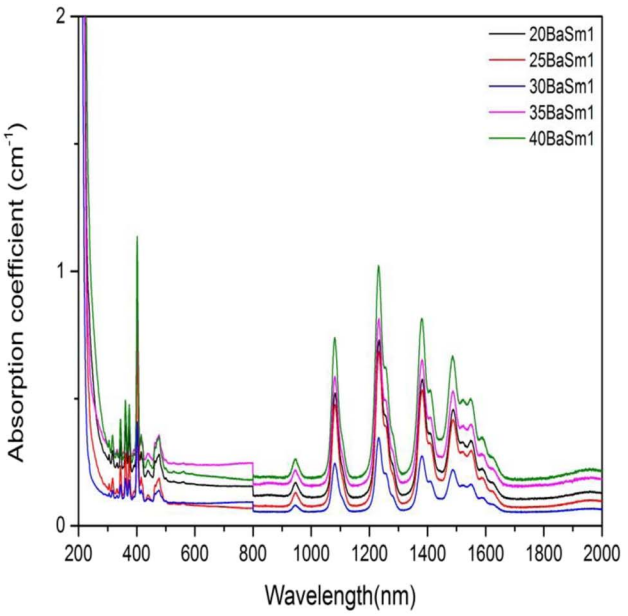

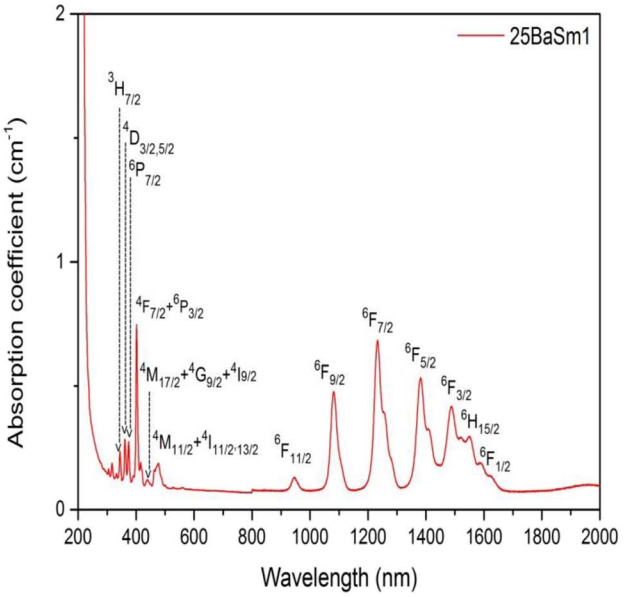

Fig. 4 The absorption spectra of series B glasses for (a) all concentrations and (b) 25 mol% of BaO and 1 mol% of Sm_2O_3.

any absorption transition may be determined by determining the absorbance of each band as follow:[35]

$$f_{exp} = 4.318 \times 10^{-9} \int \varepsilon(v) dv, \quad (3)$$

Here $\varepsilon(v)$ represents the molar absorption coefficient and can be estimated by Beer–Lambert's equation. Table 3 provides the experimental and calculated oscillator strengths for electronic transition observed in the absorption analysis. The reported values indicate that the oscillator strength values are approximately similar for most of the bands. This suggests that the non-symmetric component of the electric field acting on the Sm^{3+} ions in the glasses is nearly identical for the majority of the transitions. In addition, the transition from $^6H_{5/2}$ to $^6F_{9/2}$ located at 1079 nm with the highest magnitude of f_{exp} and f_{cal}, is considered as the hypersensitive transition.[36] Table 4 lists the Judd–Ofelt (JO) parameters obtained in this study and compare them with those reported for Sm^{3+}-doped glass materials. As seen from Table 4, the magnitude of trends of Ω_y parameters for BaSm0.3 glasses follow the order $\Omega_4 > \Omega_6 > \Omega_2$. In general, the magnitude of the Ω_2 parameter is influenced by the local structure and asymmetry surrounding the RE ions, with a strong dependence on the covalency between RE^{3+} ions and their ligand anions. The values of Ω_4 and Ω_6 are associated with the viscosity of the glass matrix and the vibronic transitions of the RE ions bound to the ligand atoms.[37,38] The comparisons of Ω_2 parameter of the present glasses with other Sm^{3+} doped

Table 3 Experimental and calculated oscillator strengths ($\times 10^{-6}$) of phosphate glasses doped 0.3% of samarium

Transition from $^6H_{5/2}$ to lower energy state	20BaSm0.3		25BaSm0.3		30BaSm0.3		35BaSm0.3		40BaSm0.3	
	f_{exp}	f_{cal}	f_{exp}	f_{cal}	f_{exp}	f_{cal}	f_{exp}	f_{cal}	f_{exp}	f_{cal}
$^4F_{7/2}$	1.059	0.040	1.059	0.040	1.059	0.040	1.059	0.041	1.059	0.041
$^4I_{13/2}$	1.627	1.653	1.627	1.654	1.628	1.654	1.627	1.658	1.627	1.662
$^6F_{11/2}$	3.246	3.140	3.248	3.170	3.284	3.170	3.284	3.151	3.284	3.132
$^6F_{9/2}$	5.311	5.589	5.351	5.650	5.352	5.646	5.535	5.689	5.535	5.731
$^6F_{7/2}$	3.670	3.419	3.717	3.456	3.718	3.454	3.813	3.495	3.908	3.536
$^6F_{5/2}$	0.599	0.5476	0.653	0.553	0.654	0.553	0.653	0.559	0.653	0.565
$^6F_{3/2}$	1.405	0.246	1.513	0.248	1.405	0.248	1.405	0.251	1.405	0.254
$^6H_{15/2}$	3.464	0.016	3.592	0.016	3.464	0.016	3.464	0.016	3.463	0.016

Table 4 J–O intensity parameters ($\times 10^{-20}$ cm^2) of BaSm0.3 phosphate glasses

Glass system	Ω_2	Ω_4	Ω_6	Trend of Ω_y	Ω_4/Ω_6 (χ)	Reference
20BaSm0.3	1.13	10.92	9.36	$\Omega_4 > \Omega_6 > \Omega_2$	1.166	Present
25BaSm0.3	1.13	11.04	9.46	$\Omega_4 > \Omega_6 > \Omega_2$	1.167	Present
30BaSm0.3	1.13	11.05	9.47	$\Omega_4 > \Omega_6 > \Omega_2$	1.169	Present
35BaSm0.3	1.14	11.26	9.57	$\Omega_4 > \Omega_6 > \Omega_2$	1.176	Present
40BaSm0.3	1.23	11.88	9.70	$\Omega_4 > \Omega_6 > \Omega_2$	1.224	Present
69.5 $NH_4H_2PO_4$–15Na_2CO_3 –15Ba_2CO_3–0.5Sm_2O_3	0.30	4.08	3.68	$\Omega_4 > \Omega_6 > \Omega_2$	1.94	28
NSBaP	0.33	8.60	3.92	$\Omega_4 > \Omega_6 > \Omega_2$	2.19	29

glasses show a higher value for our glasses, especially for the glasses containing 40 mol% of BaO. This suggests that the glass exhibits a highly asymmetric environment around the Sm^{3+} ions. Conversely, the glass's lasing efficiency is evaluated using the spectroscopic quality factor (χ), which is defined as the ratio of Ω_4 to Ω_6.[18] A smaller Ω_4/Ω_6 ratio indicates a more intense laser transition from the $^4G_{5/2}$ state to the $^6H_{7/2}$ state. The spectroscopic quality factor (χ) value for our glasses was found to be approximately 1.16, which is the smallest compared to the other glasses mentioned in Table 4. This shows that the closure transition is more than in other host glass. Consequently, the results show that our glasses appear to be better for the fabrication of photonic devices. Fig. 5 and 6 displays the emission spectra of series A and B glasses, respectively, collected in the range 510–750 nm with an excitation at 402 nm. The excitation wavelength matches with the $^6H_{5/2} \rightarrow {}^4F_{7/2}$ transition which shows to be the most sensitive among the absorption bands. Four emission bands, centered at 561, 598, 644, and 703 nm, have been observed for all Sm^{3+} doped glasses. They correspond to the transitions $^4G_{5/2} \rightarrow {}^6H_{5/2}$, $^4G_{5/2} \rightarrow {}^6H_{7/2}$, $^4G_{5/2} \rightarrow {}^6H_{9/2}$ and $^4G_{5/2} \rightarrow {}^6H_{11/2}$ respectively. For both Sm^{3+} concentrations, the emission spectra show that the transition $^4G_{5/2} \rightarrow {}^6H_{7/2}$ (598 nm) has maximum fluorescence intensity, which illustrates that the glasses are potential candidates for reddish-orange emission. The transition follows the selection rule of $\Delta J = \pm 1$, making it partly allowed for electric dipole (ED) transitions but primarily allowed for magnetic dipole (MD) transitions. The $^4G_{5/2} \rightarrow {}^6H_{5/2}$ transition, despite having $\Delta J = 0$, also includes a contribution from magnetic dipole (MD) transitions. On the other hand, the $^4G_{5/2} \rightarrow {}^6H_{9/2}$ and $^4G_{5/2} \rightarrow {}^6H_{11/2}$ transitions are purely allowed for electric dipole (ED) transitions. The intensity of these transitions is sensitive to the variations in the local structure surrounding the rare earth ion.[39] The electric dipole (ED) transition from $^4G_{5/2}$ to $^6H_{9/2}$ at 644 nm exhibits a higher intensity compared to the magnetic dipole (MD) transition from $^4G_{5/2}$ to $^6H_{5/2}$ at 561 nm. This suggests the presence of asymmetric sites for the Sm^{3+} ions in the glass.[40]

Although the addition of BaO induces depolymerization in the phosphate network, surprisingly, it was found that the emission intensity of series A glasses first decrease when BaO content increases from 20 to 35 mol% and then increases with the further increase in BaO concentration. On the other hand, for series B, the intensity of luminescence decreases with the

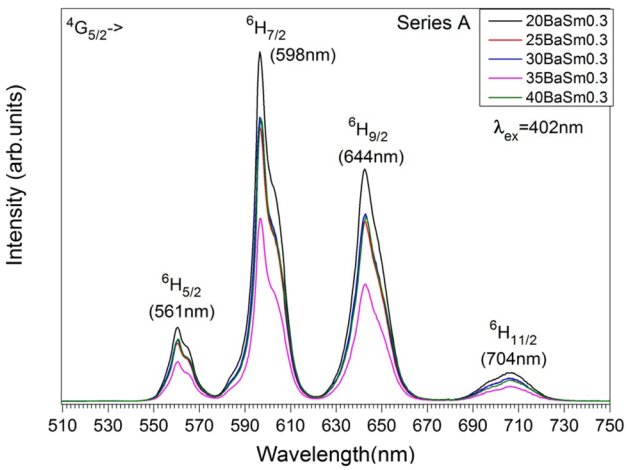

Fig. 5 The emission spectra of series A glasses.

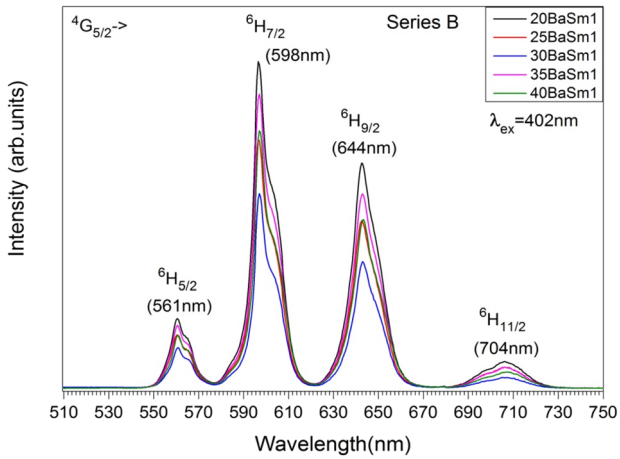

Fig. 6 The emission spectra of series B glasses.

rise of BaO concentration initially until $x = 30$, then quench up to 35 and finally decrease to 40% of BaO. Therefore, glasses with 20% BaO have the maximal luminescence intensity for series A and B. This trend correlates perfectly with the degree of polymerization in the phosphate glass. In fact, an increase in the degree of compactness and polymerization of the phosphate network leads to a corresponding rise in Sm^{3+} emission, and *vice versa*. It should be noted that an inverse trend in emission intensity is typically observed with the depolymerization of the phosphate network, as reported in earlier studies.[41,42] These results can likely be explained by the moderation of the local ligand field strength due to the modification of the glass network resulting from the replacement of Na^+ with Ba^{2+}. In this context, Na^+ cations with the higher field strength exhibit a greater preference for coordination with NBOs compared to Ba^{2+} cations. Consequently, an increase in Ba^{2+} concentration results in a decreased competition for NBO coordinations, leading to a weakening of the coordination with Sm^{3+} ions. This mechanism clearly elucidates the reduced Sm^{3+} emission observed in glasses with Ba^{2+} as network modifier ions, particularly in comparison to the relatively high field strength cations of Na^+.[43] The radiative transition probability (A_R), fluorescent branching ratio (β_R), and lifetime (τ_R) for the emission peaks of Sm^{3+} ions in the glass samples were determined using previously published equations.[40] The calculated values for the

Table 6 Lifetime values obtained under excitation at 402 nm collecting the luminescence at 598 nm

Sample	Lifetime (ms)
20BaO_Sm 0.3%	2.69
25BaO_Sm 0.3%	2.69
30BaO_Sm 0.3%	2.68
35BaO_Sm 0.3%	2.67
40BaO_Sm 0.3%	2.64
20BaO_Sm1%	1.15
25BaO_Sm1%	1.14
30BaO_Sm1%	1.15
35BaO_Sm1%	1.16
40BaO_Sm1%	1.15

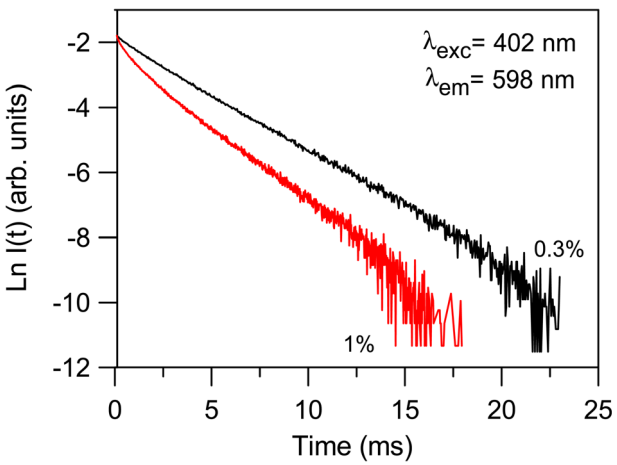

Fig. 7 Semi-logarithmic plot of the fluorescence decay of the $^4G_{5/2}$ level for the 35BaO–0.3Sm ad 35BaO–1Sm samples obtained by exciting at 402 nm and collecting the luminescence at 598 nm.

radiative transition probability (A_R) and branching ratio (β_R) for the $^4G_{5/2} \rightarrow {}^6H_{7/2}$ transition were found to be higher than those of other transitions. These values are presented in Table 5. The β_R values obtained were 0.693 for 20BaSm0.3 and 0.582 for 20BaSm1. These values indicate that our samples have a high potential to be used as a laser gain medium for 598 nm emission due to their high lasing power, low laser threshold, and

Table 5 Emission band position (λ_p, nm), radiative transition probability (A, s^{-1}), and calculated branching ratios (β_r) for the excited $^4G_{5/2}$ level of BaSm0.3 phosphate glasses

Emission transition	Transition parameters	20BaSm0.3	25BaSm0.3	30BaSm0.3	40BaSm0.3
$^4G_{5/2} \rightarrow {}^6H_{5/2}$	λ_p	561	561	561	561
	A	14.53	14.62	14.62	14.58
	β_r	0.043	0.043	0.043	0.042
$^4G_{5/2} \rightarrow {}^6H_{7/2}$	λ_p	598	598	598	598
	A	232.94	235.47	235.39	235.95
	β_r	0.693	0.695	0.695	0.694
$^4G_{5/2} \rightarrow {}^6H_{9/2}$	λ_p	644	644	644	644
	A	88.44	88.33	88.29	89.02
	β_r	0.263	0.261	0.260	0.262

Table 7 Radiatives lifetimes τ_{rad}, measured lifetimes τ_{meas} and quantum efficiencies (η)

Glass system	τ_{meas} of $^4G_{5/2}$ (ms)	τ_{rad} of $^4G_{5/2}$ (ms)	η (%)	Reference
20BaSm0.3	2.69	2.98	90.26	Present
25BaSm0.3	2.69	2.95	91.18	Present
30BaSm0.3	2.68	2.95	90.84	Present
35BaSm0.3	2.67	2.94	90.81	Present
40BaSm0.3	2.64	2.93	90.10	Present
69.5 $NH_4H_2PO_4$–15Na_2CO_3 –15Ba_2CO_3–0.5Sm_2O_3	2.01	3.41	58.89	28
NSBaP	1.74	2.40	72.5	29
NNS05	2.06	2.9	71	30

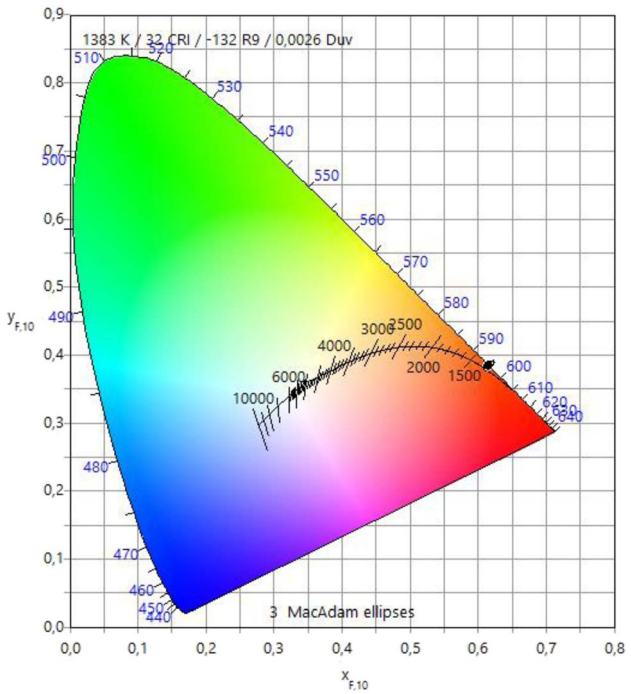

Fig. 8 CIE chromaticity diagram of the prepared glasses.

Table 8 The CIE chromaticity coordinates (*x*, *y*) and associated color temperatures (CCT, K) of the examined glass samples

	x	*y*	CCT
20BaOSm1	0.6077	0.3916	1383
25BaOSm1	0.6057	0.3934	1401
30BaOSm1	0.6044	0.3942	1411
35BaOSm1	0.6075	0.3918	1385
40BaOSm1	0.6091	0.3902	1370

suitability for laser applications.[44,45] The obtained luminescence lifetimes of the $^4G_{5/2}$ level of the glass samples are gathered in Table 6. The luminescence decays were measured by exciting the samples at 402 nm and collecting the emitted light at 598 nm. As an illustration, Fig. 7 exhibits the experimental decay curves for the 35BaO–0.3Sm and 35BaO–1Sm samples. The decays of the samples doped with 0.3 mol% of Sm^{3+} can be reasonably approximated by single exponential functions. In contrast, the decays of the samples doped with 1 mol% of Sm^{3+} deviate from a single exponential function and exhibit a reduction in lifetimes. The lifetime values in Table 6 for our compounds doped with 1 mol% represents the average lifetime, investigated using the eqn (4):

$$\langle\tau\rangle = \frac{\int_0^\infty tI(t)\mathrm{d}t}{\int_0^\infty I(t)\mathrm{d}t} \quad (4)$$

where, $I(t)$ is the luminescence intensity at time t corrected for the background. As shown in Table 6, lifetime values in glasses doped with 1 mol% Sm_2O_3 are smaller than those in the 0.3 mol% counterparts, which can be due to concentration quenching effects. However, it is noteworthy that the emission lifetime values of the $^4G_{5/2}$ level are comparable to the maximum values reported in the literature for similar concentrations of Sm^{3+} ions in glass systems,[46,47] underscoring the efficiency of the re-melting process. Specifically, the reduced presence of hydroxyl groups leads to a decrease in possible non-radiative relaxation processes for Sm^{3+} ions, thereby extending the lifetime duration. On the other hand, there are not significant differences in the lifetime values from the BaO/Na_2O substitution. Shortened lifetimes and deviation from a single exponential function are characteristic of the presence of a concentration extinction mechanism in the lifetime of $^4G_{5/2}$ level as concentration rises. The experimental decay time of the $^4G_{5/2}$ level is determined by a combination of probabilities for both radiative and nonradiative processes. Non-radiative phenomena comprise non-radiative multiphonon relaxation and cross-relaxation energy transfer, as well as impurity-induced quenching. Considering the significant energy difference of approximately 7000 cm^{-1} between the $^4G_{5/2}$ and the immediately lower level $^6F_{11/2}$, it is anticipated that non-radiative decay *via* multiphonon emission would be minimal. Hence, the decrease in lifetime with increasing concentration can be primarily attributed to cross-relaxation energy transfer processes such as ($^4G_{5/2}$; $^6H_{5/2}$) → ($^6F_{11/2}$; $^6F_{5/2}$) and ($^4G_{5/2}$; $^6H_{5/2}$) → ($^6F_{9/2}$; $^6F_{7/2}$).[18,48] The values of radiative lifetime decrease from 2.98 to 2.93 for 20BaSm0.3 and 40BaSm0.3 glass respectively. It is clear that the $^4G_{5/2}$ level's radiative lifetime was continuously longer than the observed lifetime, which gets smaller as Sm^{3+} concentration rises. This decrease can be attributed to non-radiative energy transfer processes. Table 7 presents a comparison of the quantum efficiency (η) values of the glass samples with the values reported above. The results

show that the η values for the $^4G_{5/2}$ level of the 30BaSm0.3 glass are higher than for the other glasses. Based on the obtained lifetime and quantum efficiency results, we conclude that they are promising and serve as a foundation for the development of efficient red luminophores suitable for display and illumination applications.

Fig. 8 depicts the variations in luminescent colors of the glass samples, analyzed using the Commission Internationale de l'Eclairage 1931 (CIE) chromaticity diagram. The CIE chromaticity coordinates (x, y) and associated color temperatures (CCT, K) of the examined glass samples have been computed and tabulated in Table 8. Upon substituting Na_2O with BaO content, all glass samples exhibit a nearly identical red color, showcasing prominent reddish-orange tints with CIE coordinates. Additionally, they demonstrate lower CCT values corresponding to the temperature of the closest Planckian blackbody radiator to the operating point on the chromaticity diagram.[49] These findings strongly indicate the potential of the examined glasses as phosphors, generating reddish-orange light for solid-state devices.

4. Conclusions

In summary, this investigation explored the impact of barium and samarium oxide additions on the physical, thermal, optical and luminescence characteristics of metaphosphate glasses. The density and refractive index of glass compounds rise with increasing BaO element. Furthermore, the properties values for the glasses doped with 1 mol% Sm_2O_3 are found to be higher than those of glasses doped with 0.3 mol% Sm_2O_3. The glass transition and dilatometric softening temperatures increased when BaO was substituted for Na_2O, while the coefficient of thermal expansion decreased. The analysis of FTIR spectra indicates an increasing network depolymerization with the BaO addition, with a transition from a modifier oxide to a glass-forming element for high BaO levels. The absorption spectral profiles of the glass samples exhibit similar characteristics, with the only variation being the intensities of the bands. The photoluminescence emission of BaSm0.3 glasses has higher intensity than the BaSm1 glasses, which shows that BaSm0.3 glasses have less non-radiative energy transfer processes. Moreover, the emission spectra of all glasses presented a strong reddish orange emission at 598 nm, under 402 nm excitation, with the highest intensity for the glasses with 20 mol% of BaO. Finally the lifetime of the $^4G_{5/2}$ level show similar values with the rise of BaO content and decreases with increasing Sm_2O_3 content mainly attributed to the existence of cross-relaxation processes. Further, the method used for dehydroxylation of the glasses increased the lifetimes which is the result of a strong reduction in non-radiative relaxation mechanism involving OH groups. It is concluded that current glasses may be a good candidate for displaying colors or visible lasers in the red-orange spectral region.

Data availability

The datasets generated or analyzed during the current study are available from the corresponding author on reasonable request.

Conflicts of interest

The authors declare that they have no known competing financial interests or personal relationships that could have appeared to influence the work reported in this paper.

Acknowledgements

The authors thank funding through projects MAT2017-87035-C2-1-P/-2-P from Agencia Estatal de Investigación, PID2020-115419GB-C21/C22 from Agencia Estatal de Investigación MCINN/AEI/10.13039/501100011033 and PIBA18-24 (Basque Country Government). The researchers would like to acknowledge Deanship of Scientific Research, Taif University.

References

1 A. H. Almuqrin, A. Kumar, J. F. M. Jecong, N. Al-Harbi, E. Hannachi and M. I. Sayyed, *Optik*, 2021, **247**, 167792.
2 N. Alharbiy, Z. Y. Khattari, Y. S. Rammah and A. Saleh, *J. Mater. Sci.: Mater. Electron.*, 2023, **34**, 191.
3 G. R. Dillip, C. M. Reddy, M. Rajesh, S. Chaurasia, B. D. P. Raju and S. W. Joo, *Bull. Mater. Sci.*, 2016, **39**, 711–717.
4 M. Rajesh, T. Gowthami, N. J. Sushma, B. Kamala and B. D. P. Raju, *Infrared Phys. Technol.*, 2018, **90**, 221–229.
5 N. Srinivasa Rao, M. Rajesh, S. Kumaresan, G. Rajasekhara Reddy, K. Prasad, B. Deva Prasad Raju and S. Dhanapandian, *Appl. Phys. A*, 2020, **126**, 1–6.
6 S. S. Hajer, M. K. Halimah, Z. Azmi and M. N. Azlan, *Chalcogenide Lett.*, 2014, **11**, 553–566.
7 N. Chanthima, Y. Tariwong, M. Djamal and J. Kaewkhao, *Mater. Today*, 2018, **5**, 15034–15039.
8 P. Laporta, S. Taccheo, S. Longhi, O. Svelto and C. Svelto, *Opt. Mater.*, 1999, **11**, 269–288.
9 K. Nanda, R. S. Kundu, I. Pal, R. Punia and N. Kishore, *J. Alloys Compd.*, 2016, **676**, 521–526.
10 G. Pal Singh and D. P. Singh, *J. Mol. Struct.*, 2012, **1012**, 137–140.
11 H. Mrabet, M. Atef and I. Khattech, *Mater. Chem. Phys.*, 2020, **239**, 122087.
12 N. Al-Harbi, M. I. Sayyed, R. Kurtulus, M. Kamışlıoğlu, A. Kumar, A. M. S. Alhuthali, T. Kavas and Y. Al-Hadeethi, *J. Mater. Sci.: Mater. Electron.*, 2021, **32**, 11649–11665.
13 N. Al-Harbi, M. I. Sayyed, A. Kumar, K. A. Mahmoud, O. I. Olarinoye, A. M. S. Alhuthali and Y. Al-Hadeethi, *J. Mater. Sci.: Mater. Electron.*, 2021, **32**, 12371–12382.
14 S. Jiang, T. Luo, B. Hwang and F. Smekatala, *J. Non-Cryst. Solids*, 2000, **263–264**, 364–368.
15 M. G. Mesko and D. E. Day, *J. Nucl. Mater.*, 1999, **273**, 27–36.
16 M. N. Rahaman, D. E. Day, B. S. Bal, Q. Fu, S. B. Jung, L. F. Bonewald and A. P. Tomsia, *Acta Biomater.*, 2011, **7**, 2355–2373.
17 I. Jlassi, S. Mnasri and H. Elhouichet, *J. Lumin.*, 2018, **199**, 516–527.
18 B. N. Naick, V. R. Prasad, S. Damodaraiah, A. V Reddy and Y. C. Ratnakaram, *Opt. Mater.*, 2019, **88**, 7–14.

19 S. Hussain, R. J. Amjad, M. Tanveer, M. Nadeem, H. Mahmood, A. Sattar, A. Iqbal, I. Hussain, Z. Amjad, S. Z. Hussain, S. A. Siddique and M. R. Dousti, *Glass Phys. Chem.*, 2017, **43**, 538–547.
20 A. Herrmann, S. Kuhn, M. Tiegel, C. Rüssel, J. Korner, D. Klopfel, J. Hein and M. C. Kaluza, *J. Mater. Chem. C*, 2014, **2**, 4328–4337.
21 A. Herrmann, M. Tewelde, S. Kuhn, M. Tiegel and C. Rüssel, *J. Non-Cryst. Solids*, 2018, **502**, 190–197.
22 S. Kuhn, M. Tiegel, A. Herrmann, C. Rüssel, S. Engel, C. Wenisch, S. Graf, F. A. Müller, J. Korner, R. Seifert, F. Yue, D. Klopfel, J. Hein and M. C. Kaluza, *J. Appl. Phys.*, 2015, **118**, 103104–103109.
23 F. Muñoz and R. Balda, *Int. J. Appl. Glass Sci.*, 2019, **10**, 157–161.
24 H. Ebendorff-heidepriem and D. Ehrt, *Glastech. Ber. Glass Sei. Technol.*, 1995, **68**, 139–146.
25 H. Ebendorff-Heidepriem, W. Seeber and D. Ehrt, *J. Non-Cryst. Solids*, 1993, **163**, 74–80.
26 M. Ennouri, L. Kuusela, J. Ifa, B. Gelloz, L. Petit and H. Elhouichet, *Materials*, 2019, **12**, 3516.
27 I. Konidakis, C.-P. E. Varsamis, E. I. Kamitsos, D. M oncke and D. Ehrt, *J. Phys. Chem.*, 2010, **114**, 9125–9138.
28 J. A. Wilder and J. E. Shelby, *J. Am. Ceram. Soc.*, 1984, **67**, 438–444.
29 R. K. Brow, *J. Non-Cryst. Solids*, 2000, **263**, 1–28.
30 N. Chanthima, J. Kaewkhao, C. K. Jayasankar and W. Lertlop, *Mater. Today: Proc.*, 2018, **5**, 15049–15053.
31 H. A. Lorentz, *Ann. Phys.*, 1880, **245**, 641–665.
32 W. T. Carnall, P. R. Fields and K. Rajnak, *J. Chem. Phys.*, 1968, **49**, 4424–4442.
33 M. Monisha, M. S. Murari, M. I. Sayyed, K. Naregundi, N. Al-Harbi and S. D. Kamath, *J. Non-Cryst. Solids*, 2023, **599**, 121971.
34 B. M. Walsh, *Judd–Ofelt Theory: Principles and Practices*, ed. Brian M. Walsh, 2006, pp. 403–433.
35 L. Li, Z. Leng, W. Zi and S. Gan, *J. Electron. Mater.*, 2014, **43**, 2588–2596.
36 S. Chahar, V. B. Taxak, M. Dalal, S. Singh and S. P. Khatkar, *Mater. Res. Bull.*, 2016, **77**, 91–100.
37 I. Jlassi, S. Mnasri and H. Elhouichet, *J. Lumin.*, 2018, **199**, 516–527.
38 H. Largot, K. E. Aiadi, M. Ferid, S. Hraiech, C. Bouzidi, C. Charnay and K. Horchani-naifer, *Phys. B*, 2019, **552**, 184–189.
39 C. Madhukar Reddy, B. Deva Prasad Raju, N. John Sushma, N. S. Dhoble and S. J. Dhoble, *Renewable Sustainable Energy Rev.*, 2015, **51**, 566–584.
40 A. Langar, C. Bouzidi, H. Elhouichet, B. Gelloz and M. Férid, *Displays*, 2017, **48**, 61–67.
41 M. Ennouri, L. Petit and H. Elhouichet, *Opt. Mater.*, 2022, **131**, 112610.
42 L. Kuusela, A. Veber, N. G. Boetti and L. Petit, *Materials*, 2020, **13**(3), 527.
43 A. Herrmann, A. A. Assadi, R. Lachheb, M. Zekri, A. Erlebach, K. Damak, R. Maalej, M. Sierka and C. Rüssel, *Acta Mater.*, 2023, **249**, 118811.
44 N. Luewarasirikul and J. Kaewkhao, *Mater. Today: Proc.*, 2017, **4**, 6224–6233.
45 C. Bouzidi, M. Ferhi, H. Elhouichet, M. Ferid, M. Ferhi, H. Elhouichet and M. Ferid, *J. Lumin.*, 2016, **179**, 230–235.
46 R. Turki, M. Zekri, A. Herrmann, C. Rüssel, R. Maalej and K. Damak, *J. Alloys Compd.*, 2019, **806**, 1339–1347.
47 S. Ghosh and S. Jana, *J. Lumin.*, 2023, **263**, 119980.
48 S. Damodaraiah, V. Reddy Prasad and Y. C. Ratnakaram, *Luminescence*, 2018, **33**, 594–603.
49 T. Erdem, S. Nizamoglu, X. W. Sun and H. V. Demir, *Opt. Express*, 2010, **18**, 340.